 Bull. Chem. Soc. Jpn., **74**, 765—771 (2001)

Structural Study of Crystal Transition from Hexagonal to Rectangular Phase of Lignoceric Acid Monolayers

Tisato Kajiyama,* Ryota Tominaga, Ken Kojio, and Keiji Tanaka

Department of Applied Chemistry, Faculty of Engineering, Kyushu University, Fukuoka 812-8581

(Received September 11, 2000)

Crystal transition behavior of lignoceric acid (LA) monolayer was structurally investigated by electron diffraction (ED) in conjunction with scanning force microscopy (SFM). LA molecules form two-dimensional hexagonal crystallites right after one spreads a solution at the air/water interface. The hexagonal-rectangular transition of the LA monolayer was attained by two different experimental procedures: monolayer compression under an isothermal condition and monolayer cooling under an isobaric condition. In the compression process, the hexagonal and rectangular phases coexisted in the monolayer at the surface pressure, π, of 10 mN m^{-1}, which was slightly lower than the plateau pressure, and the subphase temperature of 293 K. When the π exceeded the plateau pressure, the hexagonal phase in the LA monolayer was entirely transformed to the rectangular one. High-resolution SFM showed that the crystal transition from the hexagonal to rectangular phase proceeded via a quasi-disordered phase upon compression. A similar hexagonal-rectangular transition was also observed during the monolayer cooling process at the π of 15 mN m^{-1}. Based on SFM observation, we claimed that the molecular ordering or packing state in the rectangular lattice induced by cooling was better than that by the monolayer compression. Finally, the crystal transition mechanisms for these two procedures were proposed.

Langmuir–Blodgett (LB) films, which are prepared by the successive deposition of monolayers onto solid substratum, have been used in the development of molecular electronics, non-linear optical devices, sensors, etc. Such researches have experienced exponential growth in the number of publications in the area.[1] However, it seems that the current reported capabilities of LB films are far from what are expected. This is mainly because both macroscopic and microscopic defects, which might be introduced during a film preparation process, randomly exist in those films. Hence, the most efficient way to obtain ultimate properties in their applications is to use a defect-free, or at least a defect-diminished, monolayer as a precursor of LB films. Learning how to construct a defect-free or a defect-diminished monolayer would be realized with systematic understanding of aggregation structures of monolayers at the air/water interface.

Molecular aggregation states of fatty acid monolayers have been extensively explored owing to its quite simple structure, composed of a hydrophobic alkyl tail and a hydrophilic carboxyl group.[2–12] Consequently, the phase diagram for the fatty acid monolayers at the air/water interface has emerged on the basis of fluorescence and Brewster angle microscopy.[10,13–14] Also, the recent technique of grazing-incidence X-ray diffraction have revealed the molecular packing as well as the positional and orientational correlations of molecules in all phases.[2,15–17] Authors have also reported on the aggregation states of fatty acid monolayers with various alkyl chain lengths.[18] Of these monolayers, behenic (C_{22}) and lignoceric acid (C_{24}) monolayers exhibited the crystal transition from L_2 to CS phase at a temperature which can be accessible experimentally. The L_2 phase is historically defined as a rotator phase having short-range positional order yet enough cross-sectional area to allow free rotation, whereas the CS phase is the true two-dimensional crystal with alkyl chains oriented vertically with long-range translational order. L_2 and CS phases can be crystallographically regarded as two-dimensional hexagonal and rectangular phases, respectively. Hence, the terms of "hexagonal" and "rectangular" are used hereafter in this paper. Although both phases have been well characterized by many groups, little information has been provided on its transition process. In order to construct crystalline monolayers with well-defined structure and thus control the phase, it is of pivotal importance to explicate the phase transition process.

In this study, we elucidate how the crystal transition in lignoceric acid (LA) monolayers from the L_2 to CS phase takes place during two different procedures; (1) monolayer compression under an isothermal condition and (2) monolayer cooling under an isobaric condition.

Experimental

Monolayer Preparation. Lignoceric acid (LA) purchased from Aldrich was used without further purification. Benzene of spectroscopic grade was used as a spreading solvent. A benzene solution of LA with the concentration of 3×10^{-3} M (= mol dm^{-3}) was prepared for spreading. Water (pH = 5.8) used here was house-deionized, then further purified with a Milli-QII system (Millipore Co. Ltd.) with the initial resistivity greater than 16 MΩ. Surface pressure-area, π-A isotherm measurements and monolayer preparation were carried out with a microprocessor controlled film balance system (USI, Co., FSD-20). The surface pressure was determined by the Wilhelmy balance technique with a filter paper plate.

To examine the crystal transition behavior of the LA monolayer, two different protocols were adopted in this study. First, the

occupied area of the monolayer was varied by the continuous compression method at the speed of 120 mm^2 sec^{-1} and the T_{sp} of 293 K. The monolayer was then transferred onto a solid substrate by the vertical dipping method at a given π. The objective of the first procedure is to study the surface pressure-induced crystal transition under the isothermal condition. Second, the temperature effect on the crystal transition was examined under the isobaric condition. The monolayer was compressed up to π = 15 mN m^{-1} at the T_{sp} of 303 K, which was above the crystalline transition temperature from the hexagonal to rectangular phase, $T_{KR\text{-}KH}$, of the LA monolayer.[18] Then, the monolayer in the hexagonal crystalline state was slowly cooled down to 288 K with the cooling rate of 2 K h^{-1} at the fixed π of 15 mN m^{-1}. The change in the occupied area induced by structure relaxation[3,6] and/or crystal transition was continuously monitored during this process.

Structural Characterization of Monolayers. In order to study molecular aggregation states of a monolayer by using transmission electron microscope (TEM), the monolayer should be transferred onto a substrate without any change of aggregation state or crystallographic structure of the monolayers on the water subphase.[3] Thus, the monolayer was transferred onto the collodion-covered electron microscope grids covered with an evaporated hydrophilic SiO layer by the upward drawing method. Electron diffraction (ED) pattern of the monolayer was obtained by TEM (Hitachi H-7000), which was operated at the acceleration voltage of 75 kV and the beam current of approximately 0.5 μA. The electron beam diameter was 2.5 μm. The temperature at the sample stage of TEM was completely the same as that for the monolayer preparation.

Brewster angle IR spectroscopic measurement[19–20] was performed to evaluate molecular aggregation state of the monolayer transferred onto a piece of mica. The incident angle of p-polarized infrared beam was 54.7° so as to eliminate the multiple reflection of the infrared beam within the mica substrate. The spectrum was recorded at the resolution of 2 cm^{-1} with Nicolet Magna 860 which was equipped with a mercury–cadmium–tellin (MCT) detector. In order to obtain the spectrum with a high signal-to-noise ratio, 256 scans were collected.

Surface morphology and local mechanical properties of the monolayer were examined by a scanning force microscope (SFM; Seiko Instrument Inc., SPA 300). A Si_3N_4 tip on a cantilever with the nominal spring constant of 0.02 N m^{-1} was used. The normal force for SFM was kept as small as possible to avoid scratching the monolayer.

Results and Discussion

I. Crystal Transition by Monolayer Compression at Constant Subphase Temperature. Figure 1 shows the surface pressure-area (π-A) isotherm of the LA monolayer at the T_{sp} of 293 K, which is slightly below the $T_{KR\text{-}KH}$ of 295 K.[18] The ED patterns of the transferred LA monolayers at π = 5, 10, and 15 mN m^{-1} are also inserted in Fig. 1. The π abruptly increased with decreasing occupied area when the area reached around 0.26 nm^2 $molecule^{-1}$. Beyond the plateau pressure of approximately 12 mN m^{-1}, the π kept increasing until the monolayer collapsed. Since this is a characteristic behavior for crystalline monolayers, it is clear that crystalline domains are formed even at π = 0 mN m^{-1}.[2]

The ED pattern of the LA monolayer transferred at π = 5

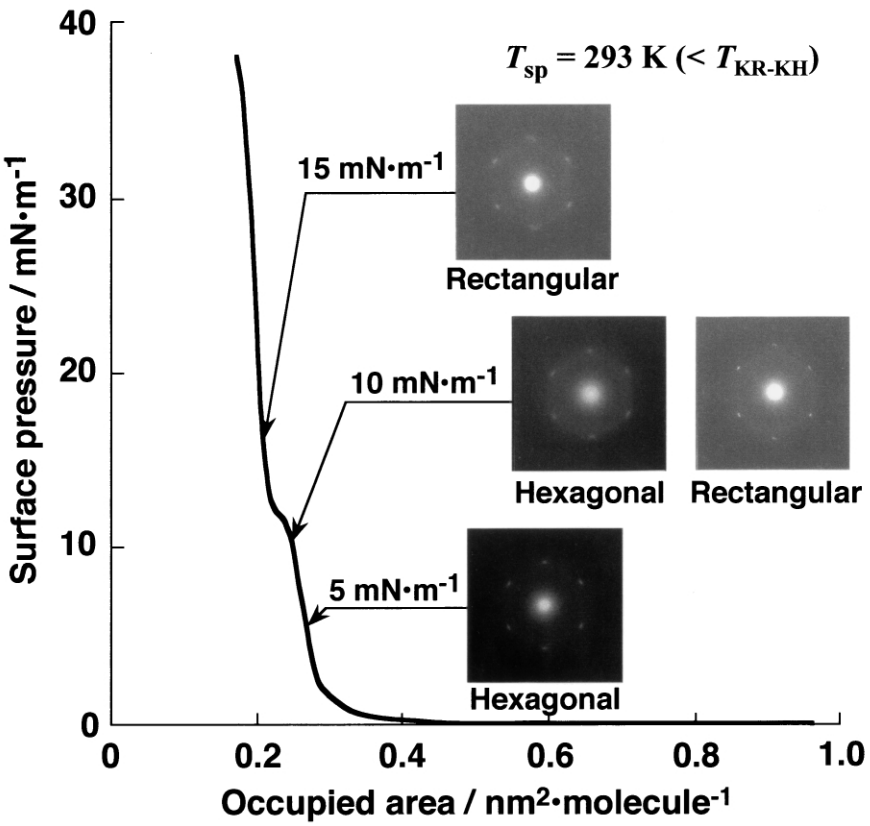

Fig. 1. π-A isotherm of LA monolayer at T_{sp} of 293 K. ED patterns of the monolayers at π = 5, 10, and 15 mN m^{-1} are also shown in it.

mN m^{-1} exhibited the sharp hexagonal crystalline spots. The (10) spacing from this ED pattern was calculated to be 0.42 nm. In contrast, in the case of the LA monolayer transferred at π = 10 mN m^{-1}, which was slightly below plateau pressure, each ED pattern showed either hexagonal or rectangular spots, as shown in Fig. 1, depending on where the observation area was. Thus, it seems reasonable to consider that the hexagonal and rectangular arrays coexist in the monolayer at π = 10 mN m^{-1}. That is, the crystal transition starts to be induced even before reaching the plateau pressure under the current condition, at the compression rate of 120 mm^2 s^{-1} and the T_{sp} of 293 K. The (20) and (11) spacings for the rectangular lattice were calculated to be 0.38 and 0.42 nm, respectively. The LA monolayer transferred at π = 15 mN m^{-1}, which was well above the plateau pressure, exhibited the ED pattern only with rectangular spots. Both the (20) and (11) spacings for this monolayer were the same as those at π = 10 mN m^{-1}.

In order to discuss the crystal transition in more detail, infrared spectroscopy was applied to the LA monolayers. Figure 2 shows the wavenumber variation of the antisymmetric stretching ($\nu_a(CH_2)$) band corresponding to alkyl tails with the occupied area. The π–A relation is shown in Fig. 2 as well. It has been reported that the peak position of the $\nu_a(CH_2)$ band for alkyl chains with zigzag conformation in an alkane single crystal is 2917 cm^{-1}.[21] Also, the corresponding $\nu_a(CH_2)$ band for the rectangular lattice appeared at 2916 cm^{-1}.[21] As shown in Fig. 2, the wavenumber of the $\nu_a(CH_2)$ band gradually shifted to smaller value upon compression via the plateau wavenumber, which was concurrently observed with the plateau pressure. Since the wavenumber of the $\nu_a(CH_2)$ band ranged from 2916.2 to 2915.3 cm^{-1} upon compression, it seems most likely that the trans population of alkyl tails is extremely high, independent of the magnitude of π. The relation between occupied area and wavenumber for the symmetric stretching band was similar to that of the $\nu_a(CH_2)$ band. The above-mentioned results are in good agreement with the ED results that the LA monolayer undergoes a crystal transition from the hexagonal to rectangular during the compression process at the T_{sp} of 293 K.

The molecular arrangement of the LA monolayer was directly observed by the aid of scanning force microscopy. Figure 3 shows the high-resolution AFM images of the LA monolayers transferred at π = (a) 5, (b) 10, and (c) 15 mN m^{-1}. The observation temperature was controlled to be the same as that for the monolayer preparation, 293 K. Since the spacing calculated from two-dimensional fast Fourier transforms of the AFM images was in good accordance with that obtained by

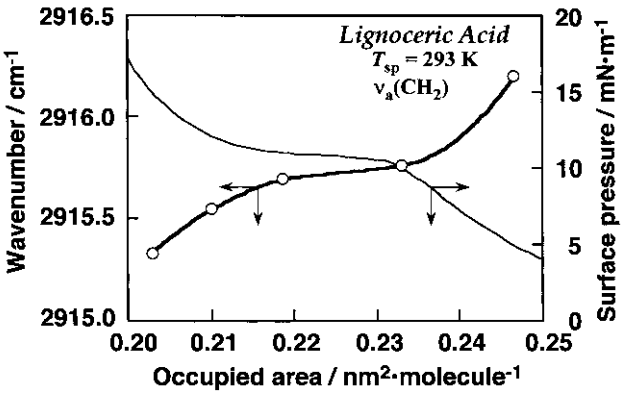

Fig. 2. Relation between occupied area and wavenumber of the antisymmetric stretching ($\nu_a(CH_2)$) band of alkyl chains of the LA molecules. The surface pressure trace with changing occupied area is shown as well.

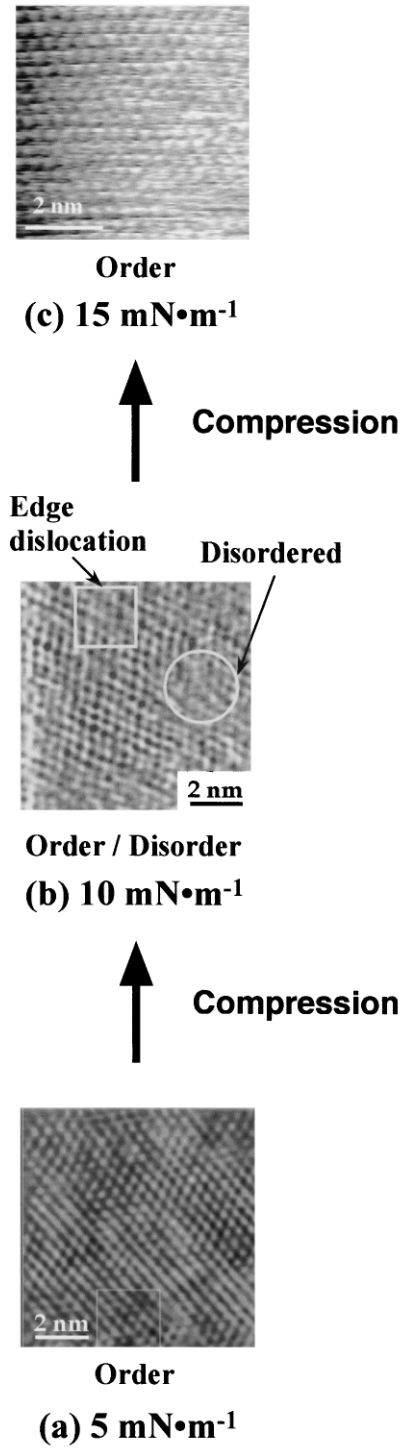

Fig. 3. High-resolution AFM images of the LA monolayers transferred at π = 5, 10, and 15 mN m^{-1} during the continuous compression process at T_{sp} = 293 K.

ED measurement, it is clear that the brighter, namely higher, portions in the AFM images correspond to individual methyl end groups of LA molecules in the monolayer. In the cases of the LA monolayers transferred at π = 5 and 15 mN m^{-1}, the well-ordered hexagonal and rectangular phases were observed, respectively, whereas the AFM image of the monolayer transferred at π = 10 mN m^{-1} showed a hexagonal lattice structure with many edge dislocations as well as disordered regions, depending on the observation area, as shown in Fig. 3b. Therefore, Fig. 3 makes it clear that the hexagonal-rectangular transition of the LA monolayer proceeds through the formation of disordered molecular arrangement.

Next, we tried to distinguish the ordered and disordered regions with respect to mechanical properties such as lateral force. Hence, LFM observation was applied to the LA monolayers, focusing on how the lateral force image changes during the crystal phase transition process. Figure 4 shows AFM and LFM images of the LA monolayers transferred at π = (a) 5, (b) 10, and (c) 15 mN m^{-1}. All surface morphologies of the LA monolayers were fairly homogeneous, independent of the magnitude of π although the bare substrate was observed as black spots. It is apparent that the area fraction of such macroscopic defects decreased by monolayer compression. The monolayer thickness determined as the step height of a hall was approximately 2.5 nm, corresponding well to the molecular length of a LA molecule in all trans conformation. No discernible contrast was observed in the LFM images of the LA monolayers transferred at π = 5 and 15 mN m^{-1} except white spots where the bare substrate was exposed, as shown in parts (a) and (c) of Fig. 4. On the other hand, the obvious contrast on the LFM image was observed in the case of the monolayer transferred at π = 10 mN m^{-1}, as shown in Fig. 4b. It has been reported that lateral force of the rectangular crystal phase is higher than that of the hexagonal one owing to the discrepancy of molecular density per unit area as well as the thermal molecular motion difference of alkyl chains.[22] As mentioned earlier, both hexagonal and rectangular phases coexisted in the LA monolayer transferred at π = 10 mN m^{-1}. Hence, it can be claimed that the contrast in Fig. 4b arises from the existence of different lattices, namely, hexagonal and rectangular, in the monolayer. On the contrary, no contrast was observed in the LFM images of the LA monolayers transferred at π = 5 and 15 mN m^{-1} because these monolayers were in the well-defined hexagonal and rectangular forms, respectively.

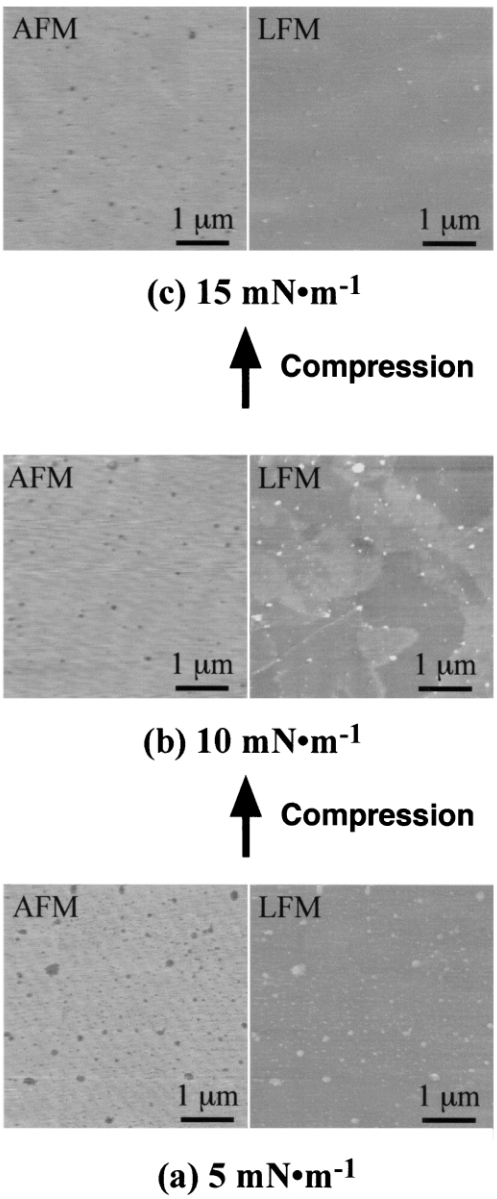

Fig. 4. Macroscopic AFM and LFM images of the LA monolayers transferred at π = 5, 10, and 15 mN m^{-1} during the continuous compression process at T_{sp} = 293 K.

II. Crystal Transition by Monolayer Cooling at Constant Surface Pressure. The crystal transition behavior of the LA monolayer induced by changing T_{sp} was examined as well. At first, the LA solution was spread at the T_{sp} of 303 K, and then the monolayer was compressed upto π = 15 mN m^{-1} under the isothermal condition. Since the T_{sp} of 303 K was above the $T_{KR\text{-}KH}$ of the LA monolayer, 295 K,[18] LA molecules in the monolayer were packed in the hexagonal array. Once the magnitude of π reached 15 mN m^{-1}, the LA monolayer

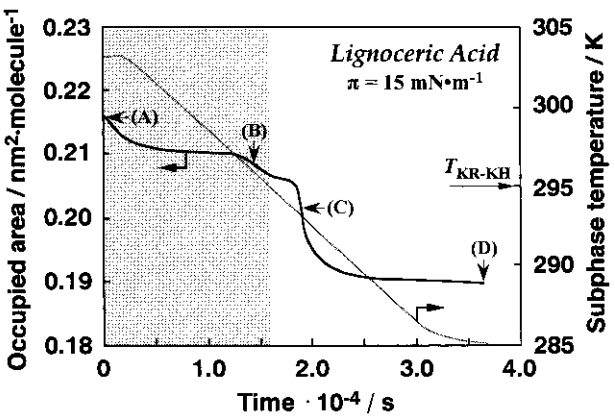

Fig. 5. Occupied area variation of the LA monolayer upon monolayer cooling, 303 to 285 K, at the constant π of 15 mN m^{-1}. The temperature trace is also shown in it. In the shaded area, the T_{sp} is higher than the $T_{KR\text{-}KH}$. The capital letters in parentheses correspond to the points, where the structural characterization was applied as shown in the next Fig. 6.

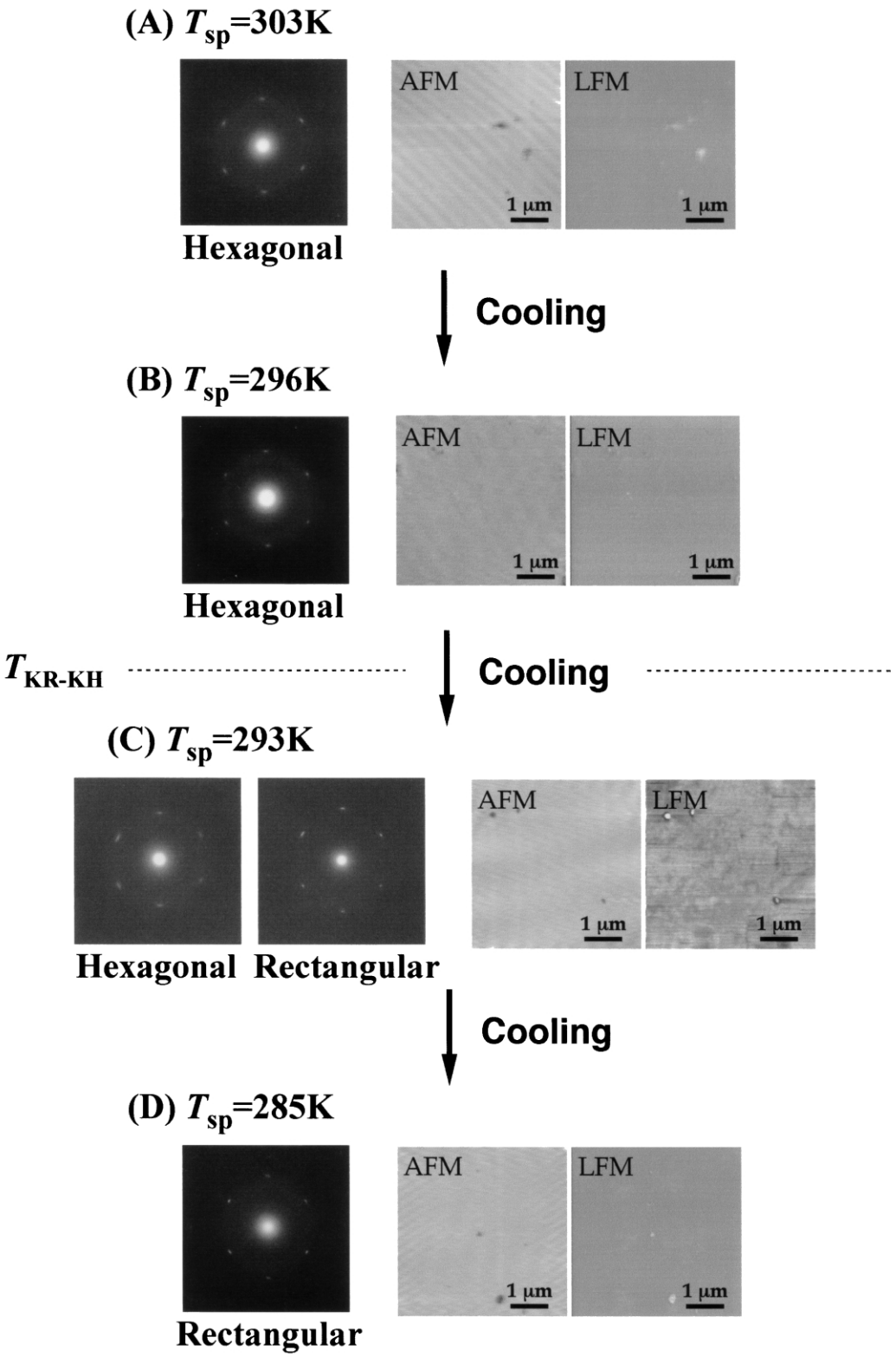

Fig. 6. ED patterns and AFM and LFM images of the LA monolayers upon monolayer cooling, 303 to 285 K, at the constant π of 15 mN m^{-1}.

started to be cooled down to 285 K at the rate of 2 K min^{-1} under the isobaric condition. Figure 5 shows the occupied area variation with the retention time for the LA monolayer during the cooling process at the fixed π of 15 mN m^{-1}. The temperature trace is also shown in Fig. 5. The left-hand and right-hand ordinates stand for the occupied area and T_{sp}, respectively. The time of 0 corresponds to the complete monolayer compression. Figure 6 shows ED patterns and AFM and LFM images of the

LA monolayers prepared at points (A), (B), (C), and (D) marked in Fig. 5. Upon monolayer cooling, the occupied area of the monolayer decreased slightly in the (A)–(B) process and drastically at 1.8×10^4 s, and then it asymptotically reached the constant occupied area of 0.19 nm^2 molecule^{-1}, as shown in Fig. 5. Since the crystal phases at points (A) and (B) were still hexagonal, as shown in Fig. 6, it is plausible that the first and second decreases in the occupied area around (A) and (B) points can be attributed to the structural relaxation of the hexagonal phase of the LA monolayer, that is, the area creep behavior.[3,6] At around (C) point, where T_{sp} passed through the $T_{KR\text{-}KH}$, the area decrement was much larger than others and ED patterns showed the coexistence of the hexagonal and rectangular phases. Hence, it seems reasonable to claim that the third decrease around (C) point can be mainly attributed to the hexagonal-rectangular phase transition. The crystallographical spacings calculated from ED patterns in Fig. 6, that is, the (10) spacing of the hexagonal lattice and the (20) and (11) spacing of the rectangular lattice, were 0.42, and 0.38 and 0.42 nm, respectively, and were the same as those of the LA monolayers upon monolayer compression at the constant subphase temperature, as mentioned above.

In contrast to surface morphologies of the LA monolayers prepared by the simple compression process shown in Fig. 4, all topographical images shown in Fig. 6 were almost perfectly homogeneous, independent of the occupied area. This means that the temperature-induced crystal transition method is superior to the surface pressure-induced crystal transition in terms of the preparation for defect-diminished monolayers. Also, no contrast was observed at all on the LFM images of the LA monolayers as long as LA molecules in the monolayer were packed either in hexagonal or rectangular arrays. On the other hand, the LFM image of the LA monolayer in the crystal transition state showed a somewhat discernible contrast, as shown in Fig. 6c. Although the heterogeneous LFM images were observed in the case of the compression-induced crystal transition, the sizes of the hexagonal and rectangular domains in the crystal transition upon monolayer cooling were smaller than those obtained by the monolayer compression process. Thus, it seems reasonable to conclude that the temperature-induced crystal transition under the isobaric condition proceeds more homogeneously than the surface pressure-induced monolayer compression under the isothermal condition.

III. Mechanism of Crystal Transition. Finally, the mechanisms of hexagonal–rectangular crystal transitions induced by both methods, monolayer compression and subphase temperature change, are proposed. Parts (a) and (b) of Fig. 7 illustrate the schematic representations of the surface pressure-induced and the temperature change-induced crystal transition behaviors. At first, it should be recalled that LA molecules form crystalline domains right after spreading a solution at the air/water interface. In monolayer compression process under the isothermal condition, crystalline domains are gathered by mechanical compression with the aid of a barrier, and then they contact one another. Such a contact point evolves into a stress concentration point. Upon further compression, the stress concentration points are successively generated, although a competitive geometrical stress relaxation proceeds. Given that the crystal transition starts to occur from a region

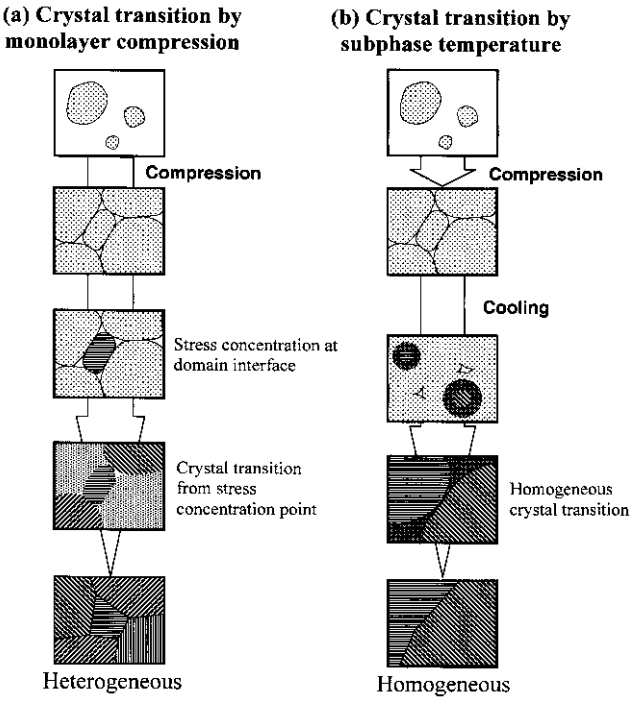

Fig. 7. Schematic representations of the crystal transition behavior induced by monolayer compression at a given temperature and monolayer cooling at a given surface pressure.

where the internal stress is relatively concentrated, it is reasonably understood that the molecular arrangement in the LA monolayer, being in the crystal transition, heterogeneously proceeds on account of the existence of many stress concentration points. On the other hand, a large homogeneous domain can be obtained by cooling a monolayer under the isobaric condition, resulting in a highly oriented molecular arrangement. Although the first process, the monolayer compression up to the 15 mN m^{-1}, is entirely the same as that of the pressure-induced crystal transition except for the magnitude of T_{sp}, the next step is totally different: the whole area of the monolayer homogeneously and slowly cooled down to a temperature below the $T_{KR\text{-}KH}$. This leads to a homogeneous crystal transition. Therefore, it seems reasonable to conclude that the molecular ordering of the two-dimensional rectangular lattice prepared by cooling the monolayer is higher than that prepared by the monolayer compression.

The molecular ordering in the monolayer formed by the compression method could be comparable or even better than that formed by changing T_{sp}, if the monolayer compression is carried out infinitely slowly. However, such a way is extremely time-consuming and unpractical for material preparation. Thus, the monolayer cooling method is more appropriate for the preparation of well-ordered two-dimensional rectangular lattices.

Conclusion

The hexagonal-to-rectangular crystal transition of the LA monolayer was structurally studied. The crystal transition was attained by two different experimental protocols: the monolay-

er compression under the isothermal condition and the temperature change under the isobaric condition. We successfully observed that the molecular rearrangement from hexagonal to rectangular phases proceeded via a disordered state. The molecular ordering of the rectangular lattice attained by the monolayer cooling under the isobaric condition was better than that obtained by another procedure.

We are most grateful for the fruitful discussions with Prof. Atsushi Takahara, Kyushu University. This study was in part supported by a Grant-in-Aid for COE Research (#08CE2005) from the Ministry of Education, Science, Sports and Culture.

References

1 A. Ulman, "An Introduction to Ultrathin Organic Thin Films from Langmuir–Blodgett to Self-Assembly," Acedmic Press, San Diego (1991).

2 P. Dutta, J. B. Peng, B. Lin, J. B. Ketterson, M. Prakash, P. Georegopoulos, and S. Ehrlich, *Phys. Rev. Lett.*, **58**, 2228 (1987).

3 T. Kajiyama, N. Morotomi, M. Uchida, and Y. Oishi, *Chem. Lett.*, **1989**, 1047.

4 K. Kjaer, J. Als-Nielsen, C. A. Helm, P. Tippman-Krayer, and H. Möhwald, *J. Phys. Chem.*, **93**, 3200 (1989).

5 C. M. Knobler, *Adv. Chem. Phys.*, **77**, 397 (1990).

6 T. Kajiyama, Y. Oishi, M. Uchida, Y. Tanimoto, and H. Kozuru, *Langmuir*, **8**, 1563 (1992).

7 T. Kajiyama Y. Oishi, M. Uchida, and Y. Takashima, *Langmuir*, **9**, 760 (1993).

8 T. Kajiyama, Y. Oishi, M. Uchida, and Y. Takashima, *Langmuir*, **9**, 1978 (1993).

9 Y. Oishi, Y. Takashima, K. Suehiro, and T. Kajiyama, *Langmuir*, **13**, 2527 (1997).

10 M. K. Durbin, A. G. Richter, C. J. Yu, J. Kmetko, J. M. Bai, and P. Dutta, *Phys. Rev. E*, **58**, 7686 (1998).

11 Y. Oishi, T. Kasagi, M. Kuramori, and K. Suehiro, *Colloid Surf., A*, **169**, 171 (2000).

12 E. Teer, C. M. Knobler, A. Braslau, J. Daillant, C. Blot, D. Luzet, M. Goldmann, and P. Fontiane, *J. Chem. Phys*. **113**, 2846 (2000).

13 G. A. Overbeck, and D. Möbius, *J. Phys. Chem*., **97**, 7999 (1993).

14 S. Riviere, S. Henon, J. Meunier, D. K. Schwartz, M.-W. Tsao, and C. M. Knobler, *J. Chem. Phys*., **101**, 10045 (1994).

15 M. C. Shih, T. M. Bohanon, J. M. Mikrut, P. Zschack, and P. Dutta, *Phys. Rev. A*, **45**, 5734 (1992).

16 I. R. Peterson, R. M. Kenn, A. Goudot, P. Fontaine, F. Rondelez, W. G. Bouwman, and K. Kjaer, *Phys. Rev. E*, **53**, 667 (1996).

17 C. Lautz, T. M. Fischer, M. Weygand, M. Losche, P. B. Howes, and K. Kjaer, *J. Chem. Phys*., **108**, 4640 (1998).

18 Y. Oishi, H. Kozuru, K. Shuto, and T. Kajiyama, *Trans. Mat. Res. Soc. Jpn.*, **15A**, 563 (1994).

19 N. J. Harrick, *Appl. Spectrosc*., **31**, 548 (1977).

20 G. Carson and Granick, *Appl. Sperctrosc.*, **43**, 473 (1989).

21 H. L.Casal, D. G. Cameron, and H. H. Mantsch, *Can. J. Chem.*, **61**, 1737 (1983).

22 K. Kojio, A. Takahara, and T. Kajiyama, *Langmuir*, **16**, 9314 (2000).